



 Cite this: *RSC Adv.*, 2020, 10, 24705

# High activity of NiCo<sub>2</sub>O<sub>4</sub> promoted Pt on three-dimensional graphene-like carbon for glycerol electrooxidation in an alkaline medium

 Bo-Cai Liu,<sup>a</sup> Shao-Li Chen,<sup>a</sup> Xiao-Yu Ling,<sup>a</sup> Qiao-Xian Li,<sup>a</sup> Chang-Wei Xu <sup>\*a</sup> and Zi-Li Liu<sup>\*b</sup>

Spinel oxide NiCo<sub>2</sub>O<sub>4</sub> supported on a three-dimensional hierarchically porous graphene-like carbon (3D HPG) material has been firstly used to enhance the activity of Pt for glycerol electrooxidation. The addition of NiCo<sub>2</sub>O<sub>4</sub> into the Pt/HPG catalyst can significantly improve the catalytic performance for glycerol oxidation. When NiCo<sub>2</sub>O<sub>4</sub> is added to the Pt/HPG catalyst, the onset potential is 25 mV more negative than that on the Pt/HPG catalyst without NiCo<sub>2</sub>O<sub>4</sub>. The current density at  $-0.3$  V on the Pt–NiCo<sub>2</sub>O<sub>4</sub> (wt 10 : 1)/HPG electrode is 1.3 times higher than that on the Pt (30 wt%)/HPG electrode. The Pt–NiCo<sub>2</sub>O<sub>4</sub> electrode presented in this work shows great potential as an electrocatalyst for glycerol electrooxidation in an alkaline medium.

 Received 26th November 2019  
Accepted 11th April 2020

DOI: 10.1039/c9ra09896h

[rsc.li/rsc-advances](http://rsc.li/rsc-advances)

## Introduction

Fuel cells are of tremendous interest from both energy and environmental consideration. Direct methanol fuel cells (DMFCs) have so many advantages that they have been extensively studied as power sources for mobile, stationary and portable applications.<sup>1,2</sup> However, the development of DMFCs is facing serious difficulties such as high methanol crossover and high toxicity of methanol. Consequently, bio-alcohols have been tendered as alternative fuels.<sup>3,4</sup> Among numerous bio-alcohols, glycerol is particularly attractive due to its high boiling point and non-toxicity compared with methanol and abundant availability in great quantities from biodiesel industry waste.<sup>5</sup> Biodiesel, a renewable vibrant biofuel, is produced from vegetable oils and animal fats by transesterification. A large amount (10% v/v) of crude glycerol is generated as a core byproduct during the synthesis of biodiesel.<sup>6</sup> Direct glycerol fuel cells show certain advantages such as low-fuel cross-over and high power density.<sup>7,8</sup> Qi *et al.* reported that direct glycerol fuel cells achieve a peak power density 276.2 mW cm<sup>-2</sup>, compared with 135.1 mW cm<sup>-2</sup> of DMFC with PdAg/CNT (0.5 mg Pd per MEA) as an anode catalyst at 353 K and ambient pressure.<sup>9</sup>

Pt-based catalysts have been investigated in depth and extensively admitted as good catalysts for glycerol electrooxidation.<sup>10–14</sup> Oxides such as MnO<sub>2</sub>, CeO<sub>2</sub>, MnO<sub>2</sub>, Mn<sub>3</sub>O<sub>4</sub>, NiO, Co<sub>3</sub>O<sub>4</sub> and TiO<sub>2</sub> have been used to enhance the activity of Pt,<sup>15–17</sup> Pd<sup>18–20</sup> and Au<sup>21–23</sup> for glycerol electrooxidation. Of all such oxides, cobalt oxide and nickel oxide have attracted considerable

attention because they can remarkably enhance the activity. The spinel oxide NiCo<sub>2</sub>O<sub>4</sub> has been used as catalyst for the electrooxidation of methanol,<sup>24–29</sup> ethanol<sup>30–32</sup> and ethylene glycol.<sup>30</sup> However, the activity of spinel oxide for alcohol electrooxidation is very low and negligible compared with that of Pt, Pd and Au. The subsequent addition of NiCo<sub>2</sub>O<sub>4</sub> into Pt, Pd and Au will lead the activity of Pt, Pd and Au to disappear for methanol and ethanol oxidation reactions.<sup>33</sup> Gao *et al.* have studied the activity of Au nanoparticle decorated NiCo<sub>2</sub>O<sub>4</sub> nanoflowers for methanol oxidation.<sup>33</sup> The onset potential ( $E_{\text{onset}}$ ) of methanol oxidation on the Au/NiCo<sub>2</sub>O<sub>4</sub> composite electrode is approximately 0.31 V (*vs.* SCE), which is close to that on the NiCo<sub>2</sub>O<sub>4</sub> (0.34 V) electrode in 1.0 mol L<sup>-1</sup> KOH with 0.5 mol L<sup>-1</sup> methanol. The peak current on the Au/NiCo<sub>2</sub>O<sub>4</sub> electrode is 1.3 times as high as that on the NiCo<sub>2</sub>O<sub>4</sub> electrode. All the results show that the activity of Au/NiCo<sub>2</sub>O<sub>4</sub> is almost the same as that of NiCo<sub>2</sub>O<sub>4</sub>.

We have reported that the spinel oxide NiCo<sub>2</sub>O<sub>4</sub> has been first used to enhance the activity of Au for glycerol electrooxidation.<sup>34</sup> The addition of NiCo<sub>2</sub>O<sub>4</sub> into the Au/HPG (hierarchically porous graphene-like carbon) catalyst can significantly improve the catalytic performance for glycerol oxidation. When NiCo<sub>2</sub>O<sub>4</sub> is added to Au/HPG, the value of  $E_{\text{onset}}$  is 108 mV more negative than that on Au/HPG. Peak current density on Au–NiCo<sub>2</sub>O<sub>4</sub> (wt 6 : 1)/HPG is 5.1 times as high as that on Au (20 wt%)/HPG. However, the value of onset potential is  $-0.255$  V (*vs.* SCE) on the Au/HPG electrode and too high for glycerol electrooxidation. The value of current density at the potential of  $-0.3$  V ( $j_{-0.3\text{V}}$ ) is 1.8 mA cm<sup>-2</sup> on the Au (20 wt%)/HPG electrode and 5.1 mA cm<sup>-2</sup> on the Au/NiCo<sub>2</sub>O<sub>4</sub> (wt 6 : 1)/HPG electrode, which is too low for fuel cells. Here, we will first use NiCo<sub>2</sub>O<sub>4</sub> to enhance the activity of Pt to get the high electrochemical performance of glycerol oxidation and also use spinel oxide to enhance the activity of Pt for alcohol electrooxidation.

<sup>a</sup>School of Chemistry and Chemical Engineering, Guangzhou University, Guangzhou 51006, China. E-mail: cw Xu@gzhu.edu.cn

<sup>b</sup>Guangzhou Key Laboratory for New Energy and Green Catalysis, Guangzhou University, Guangzhou 510006, China. E-mail: gzdxtzl@163.com



For a long time, carbon materials have been used as the supporting material for electrocatalysts of glycerol electro-oxidation.<sup>23,35</sup> As new-generation supporting materials for the electrocatalysts, graphene-based carbon materials have great advantages such as high specific active surface area, high electronic conductivity, outstanding chemical and electrochemical stability.<sup>36–38</sup> Kim *et al.* have reported very small and highly dispersed PtRu nanoparticles on a graphene support, which demonstrate excellent activity and stability compared with conventional Pt/C and bimetallic PtRu/C for glycerol electro-oxidation.<sup>39</sup> However, an irreversible aggregation or re-stacking of graphene nanosheets leads to a seriously reduced performance due to the strong van der Waals force among individual graphene nanosheets. Currently, a three-dimensional (3D) graphene architecture has been demonstrated as an effective self-supporting structure to prevent the aggregating of graphene nanosheets.<sup>40–42</sup> Shen *et al.* have developed a novel active 3D HPG material with hierarchical pores synthesized *via* an efficient ion-exchange-assisted synthesis route.<sup>40</sup> The 3D HPG material is one of numerous excellent supporting materials for electrocatalysts that provide great electrochemical stability, high electrical conductivity, controllable specific surface area as well as porous structure.<sup>43</sup> The 3D HPG material can sufficiently contact the oxide nanoparticles with a large surface area and spatial structure to availably enhance the mechanical strength of the material in suppressed volume changes, which can inhibit the aggregation of oxide nanoparticles in electrochemical reactions.<sup>44</sup> Here, we developed high performance Pt/NiCo<sub>2</sub>O<sub>4</sub> supported on 3D HPG for glycerol electrooxidation.

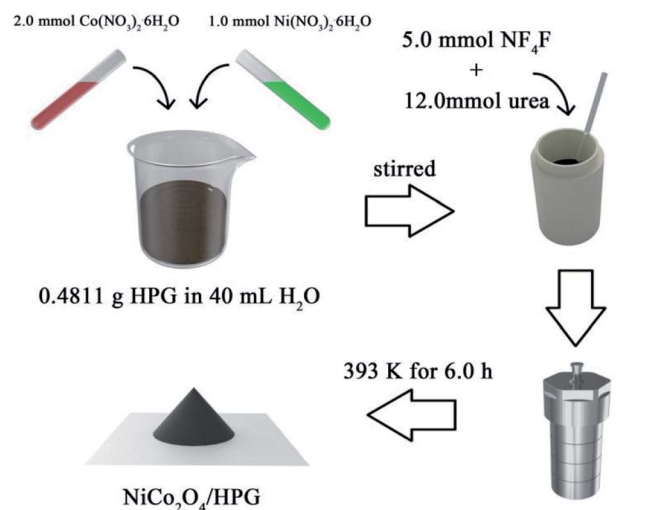
## Experimental

### Materials preparation

In this study, glycerol, KOH, Co(NO<sub>3</sub>)<sub>2</sub>·6H<sub>2</sub>O, Ni(NO<sub>3</sub>)<sub>2</sub>·6H<sub>2</sub>O solution (50 wt%), H<sub>2</sub>PtCl<sub>6</sub>·6H<sub>2</sub>O, NaBH<sub>4</sub> purchased from Aladdin were of analytical grade purity. The 3D HPG was prepared *via* a one-step ion-exchange/activation combination method according to the Li's method, and carbon precursor is a cheap metal ion exchanged resin.<sup>40,45</sup> NiCo<sub>2</sub>O<sub>4</sub>/HPG was prepared through a typical heterogeneous hydrothermal reaction method, as shown in Scheme 1. Ni(NO<sub>3</sub>)<sub>2</sub>·6H<sub>2</sub>O of 1.0 mmol, Co(NO<sub>3</sub>)<sub>2</sub>·6H<sub>2</sub>O of 2.0 mmol and 0.4811 g HPG were added into 40 mL H<sub>2</sub>O, followed by the addition of 5.0 mmol NH<sub>4</sub>F and 12.0 mmol urea. After being stirred for 1.0 h, the obtained mixture was transferred to a Teflon-lined stainless steel autoclave and heated to 393 K for 6.0 h. The resultant precipitate was washed several times with deionized water until the pH of the filtrate became 7, and then it was dried in a vacuum oven for 12.0 h. Finally, the obtained powder was annealed at 673 K for 2.0 h in air. The Pt–NiCo<sub>2</sub>O<sub>4</sub>/HPG electrocatalysts were prepared by the reduction of an H<sub>2</sub>PtCl<sub>6</sub> solution on the NiCo<sub>2</sub>O<sub>4</sub>/HPG powder using excess 0.01 mol L<sup>−1</sup> NaBH<sub>4</sub> solution.

### Electrode preparation

The electrocatalyst powders were dispersed in deionized water with 5 wt% PTFE (polytetrafluoroethylene) on the surface of



Scheme 1 Process chart of NiCo<sub>2</sub>O<sub>4</sub>/HPG preparation.

a graphite rod with a geometric area of 0.33 cm<sup>2</sup>. The loading of carbon materials and PTFE on the electrodes was accurately controlled at 0.23 and 0.1 mg cm<sup>−2</sup>. The loading of Pt on the electrodes was accurately controlled at 0.1 mg cm<sup>−2</sup>.

### Characterization

X-ray diffraction (XRD) was performed using a Panalytical X'Pert powder X-ray diffractometer with Cu K $\alpha$  radiation ( $\lambda = 0.15418$  nm) at a scan rate of 10° min<sup>−1</sup>. Scanning electron microscopy (SEM) images were recorded using a Quanta 400 FEG microscope (FEI Company). Transmission electron microscopy (TEM) images were recorded on a JEOL JEM-2010 (JEOL Ltd). Raman spectroscopy measurements were carried out on a Raman spectrometer (Renishaw Corp., UK) using a He–Ne laser with a wavelength of 514.5 nm. X-ray photoelectron spectroscopy (XPS) measurements were performed in an ESCALAB 250 spectrometer under vacuum (about  $2 \times 10^{-9}$  mbar). The percent of Pt and NiCo<sub>2</sub>O<sub>4</sub> was determined *via* ICP-MS (PerkinElmer Nexion 2000B).

All electrochemical measurements were carried out on an EG&GPAR 283 electrochemical work station (Princeton, USA) using a standard three-electrode cell in a temperature-controlled water-bath (Polyscience 9106, USA) at 298 K. Solutions were freshly prepared before each experiment. A platinum foil (3.0 cm<sup>2</sup>) was used as the counter electrode. All the potentials were measured *versus* a saturated calomel electrode (SCE, 0.241 V *vs.* SHE). A salt bridge was used between the cell and reference electrode.

## Results and discussion

Fig. 1a and b are the SEM images of 3D HPG. In Fig. 1a, there is a highly 3D connected macroporous structure. The magnified SEM (Fig. 1b) shows that there are thin layer graphene-like walls in the 3D HPG. The TEM images further show that the HPG material has an interconnected 3D porous structure network (Fig. 1c). The thin layer graphene-like wall is generally 4–6 nm

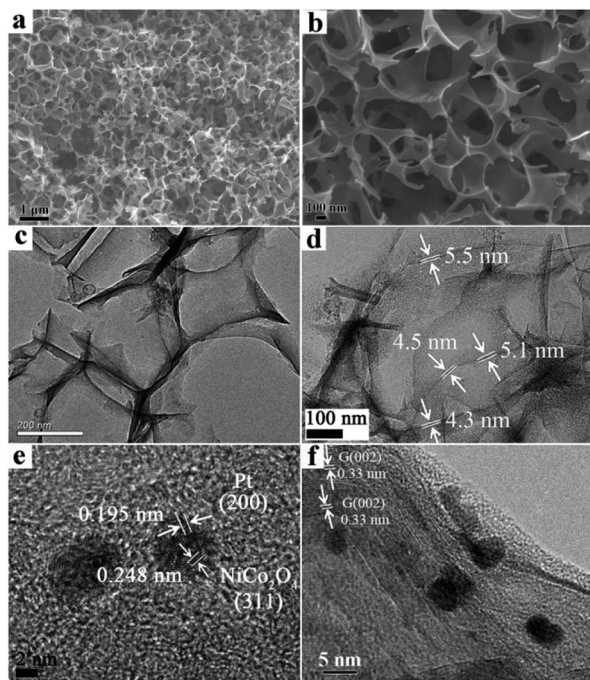


Fig. 1 (a and b) SEM images of 3D HPG, (c and d) TEM images of 3D HPG and (e and f) TEM images of Pt–NiCo<sub>2</sub>O<sub>4</sub> (wt 10 : 1)/HPG.

thick, as shown in Fig. 1d. The typical TEM images of Pt–NiCo<sub>2</sub>O<sub>4</sub> (wt 10 : 1)/HPG are shown in Fig. 1e and f. As shown in Fig. 1e, the nanoparticles of Pt and NiCo<sub>2</sub>O<sub>4</sub> can be found, and they contact each other closely. The catalyst nanoparticles fix on the surface of HPG, and their size is 3–10 nm. A parallel fringe with a spacing of 0.33 nm can be clearly observed, which corresponds to the (002) plane of graphene (Fig. 1f).

XRD patterns for NiCo<sub>2</sub>O<sub>4</sub>/HPG, Pt/HPG and Pt–NiCo<sub>2</sub>O<sub>4</sub> (wt 10 : 1)/HPG are shown in Fig. 2. A diffraction peak at around 26.2° observed in all the samples is assigned to the (002) plane of graphene. Diffraction peaks at around 31.3°, 36.6°, 44.5°, 58.6° and 65.0° are assigned to the (220), (311), (200), (511) and (440) facets of NiCo<sub>2</sub>O<sub>4</sub>. In the case of NiCo<sub>2</sub>O<sub>4</sub>/HPG and Pt–NiCo<sub>2</sub>O<sub>4</sub> (wt 10 : 1)/HPG, the XRD peaks of NiCo<sub>2</sub>O<sub>4</sub> are in good agreement with the standard card (JCPDS no. 20-0781). The strong diffraction peaks at the Bragg angles of 39.8°, 46.3°, 67.8°, 81.4° and 86.0° correspond to the (111), (200), (220), (311) and (222) facets of the face-centered-cubic (fcc) crystallite Pt. In the XRD pattern of Pt–NiCo<sub>2</sub>O<sub>4</sub> (wt 10 : 1)/HPG, the diffraction peaks of Pt and NiCo<sub>2</sub>O<sub>4</sub> can be discovered, which indicates that the Pt–NiCo<sub>2</sub>O<sub>4</sub>/HPG catalysts have been synthesized successfully.

Chemical bonding states in NiCo<sub>2</sub>O<sub>4</sub>/HPG were analyzed *via* XPS, as shown in Fig. 3. A survey spectrum is shown in Fig. 3a and the peaks are corresponding to C 1s, O 1s, Co 2p and Ni 2p. The binding energy of the C 1s peak is located at 285.2 eV, which is related to the graphitic carbon in 3D HPG, as shown in Fig. 3a. The binding energy values of the XPS spectrum of Ni 2p are 856.6 and 874.6 eV, as shown in Fig. 3c, which corresponds to Ni 2p<sub>3/2</sub> and Ni 2p<sub>1/2</sub>. It can also be assigned to Ni(II), while the satellite peaks at 862.1 and 880.6 eV are two shake-up type peaks of nickel at the high binding energy side of the Ni 2p<sub>1/2</sub>

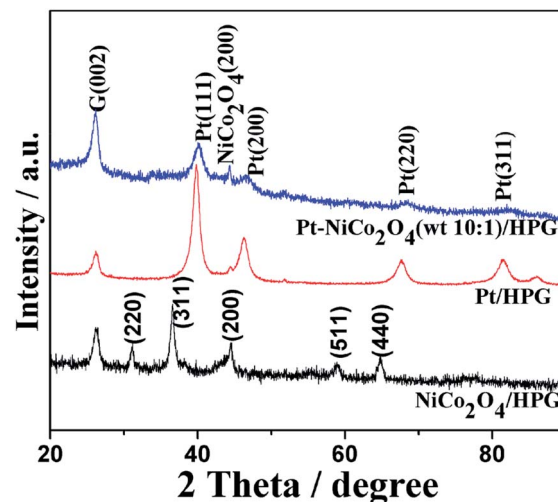


Fig. 2 XRD image for NiCo<sub>2</sub>O<sub>4</sub>/HPG, Pt/HPG and Pt–NiCo<sub>2</sub>O<sub>4</sub> (wt 10 : 1)/HPG.

and Ni 2p<sub>3/2</sub> edge.<sup>46,47</sup> The Ni 2p spectra for the two spin-orbit doublet characteristics of Ni(II) with a low content of Ni(III) are consistent with the two shake-up satellites.<sup>33,48</sup> The binding energy values of the XPS spectrum of Co 2p are 780.6 and 797.6 eV for NiCo<sub>2</sub>O<sub>4</sub>/HPG, which are assigned to Co 2p<sub>3/2</sub> and Co 2p<sub>1/2</sub>, as shown in Fig. 3d, which can prove the existence of Co(III) with a low content of Co(II).<sup>33,47</sup> The results indicate that NiCo<sub>2</sub>O<sub>4</sub>/HPG has been synthesized successfully. The chemical bonding states in Pt–NiCo<sub>2</sub>O<sub>4</sub> (wt 10 : 1)/HPG were analyzed *via* XPS, as shown in Fig. 3. A survey spectrum is shown in Fig. 3a, and the peaks correspond to Pt 4f, C 1s, O 1s, Co 2p and Ni 2p. As shown in Fig. 3b, the binding energy values of the XPS spectrum of Pt 4f are 71.6 and 74.9 eV, corresponding to Pt 4f<sub>7/2</sub> and Pt 4f<sub>5/2</sub>, which are consistent with the typical binding energy values of metallic Pt<sup>0</sup> species.<sup>49</sup> These data show that Pt specie attached to the surface of 3D HPG exists in the form of Pt<sup>0</sup>. The binding energy values of Ni 2p are 857.0 and 876.7 eV

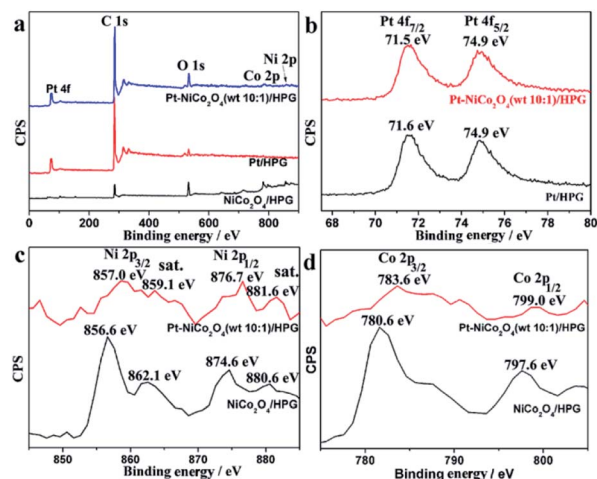


Fig. 3 XPS spectra for the Pt–NiCo<sub>2</sub>O<sub>4</sub> (wt 10 : 1)/HPG of (a) survey, (b) Pt 4f, (c) Ni 2p and (d) Co 2p.

and assigned to the Ni 2p<sub>3/2</sub> and Ni 2p<sub>1/2</sub> as shown in Fig. 3c, which can be assigned to Ni(II). The two shake-up satellites of the Ni 2p spectrum show the two spin-orbit doublet peaks of Ni(II) with a low content of Ni(III). The binding energy values of Co 2p are 783.6 and 799.0 eV and are assigned to Co 2p<sub>3/2</sub> and Co 2p<sub>1/2</sub>, respectively, as shown in Fig. 3d, which can be assigned to Co(III) with a low content of Co(II). In the XPS spectrum of Pt–NiCo<sub>2</sub>O<sub>4</sub> (wt 10 : 1)/HPG, the binding energy values of Pt and NiCo<sub>2</sub>O<sub>4</sub> can be discovered, which indicates that the Pt–NiCo<sub>2</sub>O<sub>4</sub>/HPG catalysts have been synthesized successfully.

Cyclic voltammetry (CV) measurements for glycerol electrooxidation on the NiCo<sub>2</sub>O<sub>4</sub>/HPG electrode was carried out in 1.0 mol L<sup>-1</sup> KOH containing a 1.0 mol L<sup>-1</sup> glycerol solution at a sweep rate of 5 mV s<sup>-1</sup> on the NiCo<sub>2</sub>O<sub>4</sub> electrode with a NiCo<sub>2</sub>O<sub>4</sub> loading of 0.10 mg cm<sup>-2</sup> to evaluate the activity of NiCo<sub>2</sub>O<sub>4</sub>, as shown in Fig. 4. The background is the CV measured in a nitrogen-saturated 1.0 mol L<sup>-1</sup> KOH solution without glycerol. Compared with the CV in the absence of glycerol, a glycerol oxidation peak can be clearly observed in the CV curve on the NiCo<sub>2</sub>O<sub>4</sub>/HPG electrode in the presence of 1.0 mol L<sup>-1</sup> glycerol. The value of  $E_{\text{onset}}$  is 0.232 V on the NiCo<sub>2</sub>O<sub>4</sub>/HPG electrode. This result is almost consistent with that reported by Sun *et al.* for methanol, ethanol and ethylene glycol.<sup>30,50</sup> The value of  $E_{\text{onset}}$  is about 0.48 V vs. Hg/HgO (1.0 mol L<sup>-1</sup> KOH) for ethanol and ethylene glycol, 0.536 V for methanol in 1.0 mol L<sup>-1</sup> and KOH, and 0.5 mol L<sup>-1</sup> alcohol (methanol, ethanol or ethylene glycol) at 10 mV s<sup>-1</sup>.

CV measurement for glycerol electrooxidation on the Pt–NiCo<sub>2</sub>O<sub>4</sub> (wt 10 : 1)/HPG electrode is carried out in N<sub>2</sub>-saturated 1.0 mol L<sup>-1</sup> KOH containing a 1.0 mol L<sup>-1</sup> glycerol solution at a sweep rate of 5 mV s<sup>-1</sup> at a Pt loading of 0.10 mg cm<sup>-2</sup>, as shown in Fig. 5a. The background is a CV curve in a N<sub>2</sub>-saturated 1.0 mol L<sup>-1</sup> KOH without glycerol on the Pt–NiCo<sub>2</sub>O<sub>4</sub> (wt 10 : 1)/HPG electrode. According to the eqn (1) for Pt-based catalysts using hydrogen desorption the specific electrochemical active surface area (EASA) can be calculated:<sup>51</sup>

$$\text{EASA (m}^2 \text{ g}^{-1}) = \frac{Q_{\text{H}} (\mu\text{C cm}^{-2})}{210 (\mu\text{C cm}^{-2}) \times W (\text{g cm}^{-2})} \times \frac{1 (\text{m}^2)}{10\,000 (\text{cm}^2)} \quad (1)$$

where  $W$  is the Pt loading on the electrode,  $Q_{\text{H}}$  the total charge associated with hydrogen desorption, and 210  $\mu\text{C cm}^{-2}$  is the charge corresponding to the adsorption of a monolayer of hydrogen on a polycrystalline Pt surface. The EASA value for Pt (30 wt%)/HPG is 45.1 m<sup>2</sup> g<sup>-1</sup> and that for Pt–NiCo<sub>2</sub>O<sub>4</sub> (wt 10 : 1)/HPG is 53.8 m<sup>2</sup> g<sup>-1</sup>. With the same Pt loading of 0.1 mg cm<sup>-2</sup>, the EASA value for Pt (30 wt%)/HPG is about three times as high as that for Pt (30 wt%)/C (Carbon Vulcan XC-72) (14.8 m<sup>2</sup> g<sup>-1</sup>) and Pt (27 wt%)/C (16.0 m<sup>2</sup> g<sup>-1</sup>) in our previous results.<sup>51,52</sup> The results show that 3D HPG has a high specific electrochemical active surface area. A glycerol oxidation peak can be clearly observed in the CV curve on the Pt (30 wt%)/HPG electrode in the Fig. 5a. As shown in our previous study, the activity of glycerol oxidation on the Pt (30 wt%)/HPG electrode is much higher than that on the Pt (30 wt%)/C electrode in the same condition.<sup>51</sup> The value of  $E_{\text{onset}}$  is -0.623 V on the Pt (30 wt%)/HPG electrode, which is 52 mV lower than that on the Pt (30 wt%)/C electrode (-0.571 V).<sup>51</sup> The lower value of  $E_{\text{onset}}$  shows an easier electrooxidation of glycerol. The current for glycerol electrooxidation on the Pt (30 wt%)/HPG electrode begins to rise much more sharply at a more negative potential than that on the Pt (30 wt%)/C electrode. It demonstrates that glycerol can be easily electrochemically oxidized on the Pt (30 wt%)/HPG electrode. The value of  $j_{-0.3 \text{ V}}$  is 35.9 mA cm<sup>-2</sup> on the Pt (30 wt%)/HPG electrode, and 16.3 mA cm<sup>-2</sup> on the Pt (30 wt%)/C electrode, and the former is 2.2 times as high as the latter.<sup>51</sup> The results show that HPG is a good support for electrocatalysts used for glycerol oxidation. A glycerol oxidation peak can be clearly observed in the CV curve on the Pt–NiCo<sub>2</sub>O<sub>4</sub> (wt 10 : 1)/HPG electrode. It is obvious that the activity of glycerol oxidation on the Pt–NiCo<sub>2</sub>O<sub>4</sub> (wt 10 : 1)/HPG electrode is much higher than that on the Pt (30 wt%)/HPG electrode. The value of  $E_{\text{onset}}$  is -0.648 V on the Pt–NiCo<sub>2</sub>O<sub>4</sub> (wt 10 : 1)/HPG electrode, which is 25 mV more negative compared with that on the Pt (30 wt%)/HPG electrode (-0.623 V). The current for glycerol electrooxidation on the Pt–NiCo<sub>2</sub>O<sub>4</sub> (wt 10 : 1)/HPG electrode begins to rise much more sharply at a more negative

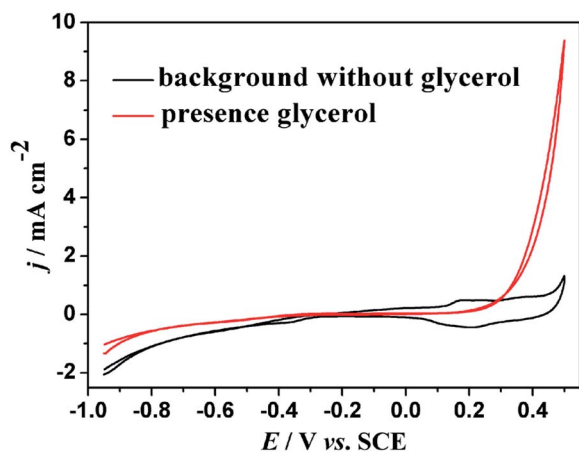


Fig. 4 CV curves on the NiCo<sub>2</sub>O<sub>4</sub>/HPG electrode in 1.0 mol L<sup>-1</sup> KOH (black line) and 1.0 mol L<sup>-1</sup> KOH containing 1.0 mol L<sup>-1</sup> glycerol (red line).

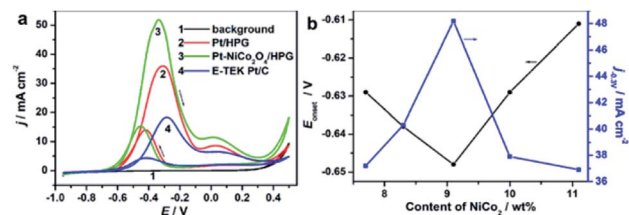


Fig. 5 (a) CV curves on Pt/HPG, Pt–NiCo<sub>2</sub>O<sub>4</sub> (wt 10 : 1)/HPG and commercial E-TEK Pt/C electrodes in 1.0 mol L<sup>-1</sup> KOH containing 1.0 mol L<sup>-1</sup> glycerol with a sweep rate of 5 mV s<sup>-1</sup>, (b) plots of  $E_{\text{onset}}$  and  $j_{-0.3 \text{ V}}$  in CV curves as a function of Pt weight percent in Pt–NiCo<sub>2</sub>O<sub>4</sub>/HPG.

potential than that on the Pt (30 wt%)/HPG electrode. It demonstrates that glycerol can be easily electrochemically oxidized on the Pt–NiCo<sub>2</sub>O<sub>4</sub> (wt 10 : 1)/HPG electrode. The value of  $j_{-0.3 \text{ V}}$  is 48.2 mA cm<sup>-2</sup> on the Pt–NiCo<sub>2</sub>O<sub>4</sub> (wt 10 : 1)/HPG electrode, which is 1.3 times as high as that on the Pt (30 wt%)/HPG electrode (35.9 mA cm<sup>-2</sup>). The results show that NiCo<sub>2</sub>O<sub>4</sub> can promote the activity of Pt for glycerol oxidation. In order to illustrate the advantage of the Pt–NiCo<sub>2</sub>O<sub>4</sub> (wt 10 : 1)/HPG electrocatalyst, the activity of glycerol oxidation on the commercial E-TEK Pt (30 wt%)/C electrode is compared with the same Pt loading of 0.1 mg cm<sup>-2</sup>. The value of  $E_{\text{onset}}$  is -0.582 V on the commercial E-TEK Pt/C electrode. The value of  $E_{\text{onset}}$  on the Pt–NiCo<sub>2</sub>O<sub>4</sub> (wt 10 : 1)/HPG electrode is 66 mV more negative compared with that on the commercial E-TEK Pt/C electrode. The value of  $j_{-0.3 \text{ V}}$  is 18.2 mA cm<sup>-2</sup> on the commercial E-TEK Pt/C electrode. The value of  $j_{-0.3 \text{ V}}$  on the Pt–NiCo<sub>2</sub>O<sub>4</sub> (wt 10 : 1)/HPG electrode is 2.6 times as high as that on the commercial E-TEK Pt/C electrode. The results show that the Pt–NiCo<sub>2</sub>O<sub>4</sub> (wt 10 : 1)/HPG gives a higher activity of glycerol electrooxidation than commercial E-TEK Pt/C.

The effects of the NiCo<sub>2</sub>O<sub>4</sub> content in the Pt–NiCo<sub>2</sub>O<sub>4</sub>/HPG electrocatalyst for glycerol oxidation was investigated in a N<sub>2</sub>-saturated 1.0 mol L<sup>-1</sup> KOH containing 1.0 mol L<sup>-1</sup> glycerol solution at a sweep rate of 5 mV s<sup>-1</sup>. Pt loading was fixed as 0.10 mg cm<sup>-2</sup>. Fig. 5b shows the plots of the value of  $E_{\text{onset}}$  and  $j_{-0.3 \text{ V}}$  as a function of NiCo<sub>2</sub>O<sub>4</sub> loading for glycerol oxidation. It can be seen that the value of  $E_{\text{onset}}$  for glycerol oxidation decreases with the increase in the oxide content in the Pt–NiCo<sub>2</sub>O<sub>4</sub>/HPG catalyst, but increases again when the value of  $E_{\text{onset}}$  reaches a minimum value. Moreover, the value of  $j_{-0.3 \text{ V}}$  for glycerol oxidation increases with an increase in the NiCo<sub>2</sub>O<sub>4</sub> content in the Pt–NiCo<sub>2</sub>O<sub>4</sub>/HPG catalysts, but decreases again when it reaches a maximum value. The best result found that the lowest value of  $E_{\text{onset}}$  and the highest value of  $j_{-0.3 \text{ V}}$  are obtained at the weight ratio of 10 : 1 for Pt to NiCo<sub>2</sub>O<sub>4</sub> in the Pt–NiCo<sub>2</sub>O<sub>4</sub>/HPG.

The chronoamperometry curves at -0.3 V for glycerol oxidation on the NiCo<sub>2</sub>O<sub>4</sub>/HPG, Pt/HPG, Pt–NiCo<sub>2</sub>O<sub>4</sub> (wt 10 : 1)/HPG and commercial E-TEK Pt/C electrodes in 1.0 mol L<sup>-1</sup> KOH containing the 1.0 mol L<sup>-1</sup> glycerol solution are shown in Fig. 6. It is well-known that some intermediate species such as CO-like species will make the current of alcohol oxidation to decrease during the alcohol oxidation process with being adsorbed on the surface of electrode. This phenomenon is directly reflected by the rapid current decay in the chronoamperometry curves, which shows the poisoning of the catalysts. The current decays rapidly on the Pt/HPG and commercial E-TEK Pt/C electrodes, while the current decays slowly on the Pt–NiCo<sub>2</sub>O<sub>4</sub> (wt 10 : 1)/HPG electrode. The results show that NiCo<sub>2</sub>O<sub>4</sub> in the Pt/HPG will enhance the discharge capacity during the glycerol oxidation process. Nevertheless, at the end of the test, the oxidation current density is 3.1 mA cm<sup>-2</sup> on the Pt–NiCo<sub>2</sub>O<sub>4</sub> (wt 10 : 1)/HPG electrode, which is larger than that on the Pt/HPG electrode (1.8 mA cm<sup>-2</sup>) and commercial E-TEK Pt/C electrode (0.6 mA cm<sup>-2</sup>).

The enhanced performance of glycerol oxidation on Pt–NiCo<sub>2</sub>O<sub>4</sub>/HPG can be attributed to a bifunctional mechanism.

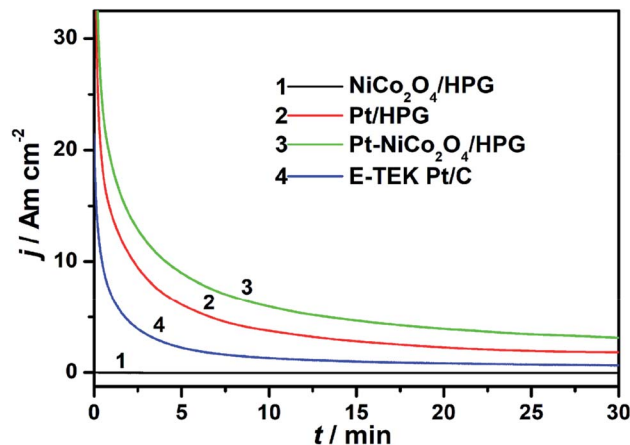


Fig. 6 Chronoamperometry curves on NiCo<sub>2</sub>O<sub>4</sub>/HPG, Pt/HPG, Pt–NiCo<sub>2</sub>O<sub>4</sub> (wt 10 : 1)/HPG and E-TEK Pt/C electrodes in 1.0 mol L<sup>-1</sup> KOH containing 1.0 mol L<sup>-1</sup> glycerol at a potential of -0.3 V.

The reaction intermediate species and products of glycerol electrooxidation on the Pt electrode are glyoxylic acid, tartaric acid, glycolic acid, formic acid, dihydroxyacetone, carbon dioxide, and so forth.<sup>53,54</sup> *In situ* Fourier transform infrared (FTIR) shows that the intermediate species on the surface of electrode in an alkaline medium during glycerol electrooxidation are acyl species (-CO<sub>ads</sub>), which can be strongly adsorbed on the surface of electrode.<sup>55</sup> The acyl intermediate species can be adsorbed on the surface of the Pt electrode by the coordination with the metal through the carbon of the carbonyl group. It is believed that oxides such as NiCo<sub>2</sub>O<sub>4</sub> have capacity to generate active oxygen-containing species (OH<sub>ads</sub>) on the Pt surface at a lower potential. OH<sub>ads</sub> at a lower potential can transform reaction intermediate species on the surface of Pt nanoparticles to dissolved species in water, releasing the active sites on the surface of Pt for further electrochemical reactions, as shown in eqn (2) and (3).



## Conclusions

In summary, a novel active three-dimensional hierarchically porous graphene-like carbon (3D HPG) material with hierarchical pores was synthesized *via* an efficient ion-exchange-assisted synthesis route. The results show that HPG is a good support for electrocatalysts for glycerol oxidation. It is obvious that the activity of glycerol oxidation on the Pt (30 wt%)/HPG electrode is much higher than that on the Pt (30 wt%)/C (Carbon Vulcan XC-72) electrode. The results indicate that the addition of NiCo<sub>2</sub>O<sub>4</sub> into the Pt/HPG catalyst can significantly improve the catalytic performance of glycerol oxidation. When NiCo<sub>2</sub>O<sub>4</sub> is added to the Pt/HPG, the value of  $E_{\text{onset}}$  is 25 mV more negative than that on the pure Pt/HPG catalyst. The value of  $j_{-0.3 \text{ V}}$  on the Pt–NiCo<sub>2</sub>O<sub>4</sub> (wt 10 : 1)/HPG electrode is 1.3

times as high as that on the Pt (30 wt%)/HPG electrode. The activity and stability of glycerol oxidation on Pt/HPG are promoted obviously by the addition of NiCo<sub>2</sub>O<sub>4</sub>. The Pt–NiCo<sub>2</sub>O<sub>4</sub> presented in this work shows great potential as an excellent electrocatalyst for glycerol electrooxidation in an alkaline medium in direct glycerol fuel cells.

## Conflicts of interest

There are no conflicts to declare.

## Acknowledgements

This work was financially supported by National Natural Science Foundation of China (21676060), the Natural Science Foundation of Guangdong Province (2014A030313521), Scientific Research Foundation for Yangcheng Scholar (1201561607), Science and Technology Program of Guangzhou (201510010112, 201704020005).

## Notes and references

- 1 M. M. Shahid, A. Pandikumar, A. M. Golsheikh, N. M. Huang and H. N. Lim, *RSC Adv.*, 2014, **4**, 62793–62801.
- 2 T. Z. Huang, S. Mao, G. H. Zhou, Z. L. Zhang, Z. H. Wen, X. K. Huang, S. Q. Ci and J. H. Chen, *Nanoscale*, 2015, **7**, 1301–1307.
- 3 J. T. Zhong, D. Bin, B. Yan, Y. Feng, K. Zhang, J. Wang, C. Q. Wang, Y. Shiraishi, P. Yang and Y. K. Du, *RSC Adv.*, 2016, **6**, 72722–72727.
- 4 B. Habibi and N. Delnavaz, *RSC Adv.*, 2016, **6**, 31797–31806.
- 5 A. Zalineeva, A. Serov, M. Padilla, U. Martinez, K. Artyushkova, S. Baranton, C. Coutanceau and P. B. Atanassov, *Appl. Catal., B*, 2015, **176–177**, 429–435.
- 6 M. S. Rahman, C. B. Xu, K. S. Ma, H. P. Guo and W. S. Qin, *Renewable Energy*, 2017, **114**, 1272–1280.
- 7 A. N. Geraldes, D. F. Silva, L. G. A. Silva, E. V. Spinacé, A. O. Neto and M. C. Santos, *J. Power Sources*, 2015, **293**, 823–830.
- 8 N. Benipal, J. Qi and J. C. Gentile, *Renewable Energy*, 2017, **105**, 647–655.
- 9 J. Qi, N. Benipal, C. H. Liang and W. Z. Li, *Appl. Catal., B*, 2016, **199**, 494–503.
- 10 L. Huang, J. Y. Sun, S. H. Cao, M. Zhan, Z. R. Ni, H. J. Sun, Z. Chen, Z. Y. Zhou, E. G. Sorte, Y. J. Tong and S. G. Sun, *ACS Catal.*, 2016, **6**, 7686–7695.
- 11 A. J. Xie, F. Tao, L. N. Hu, Y. F. Li, W. L. Sun, C. Jiang, F. F. Cheng, S. P. Luo and C. Yao, *Electrochim. Acta*, 2017, **231**, 502–510.
- 12 E. Habibi and H. Razmi, *Int. J. Hydrogen Energy*, 2012, **37**, 16800–16809.
- 13 E. Antolini, *Catalysts*, 2019, **9**, 980.
- 14 M. B. C. de Souza, V. Y. Yukuhiro, R. A. Vicente, C. T. G. V. M. T. Pires, J. L. Bott-Neto and P. S. Fernández, *ACS Catal.*, 2020, **10**, 2131–2137.
- 15 A. C. Garcia, E. B. Ferreira, V. V. S. Barros and J. J. Linares, *J. Electroanal. Chem.*, 2017, **793**, 188–196.
- 16 C. W. Xu, R. Zeng, P. K. Shen and Z. D. Wei, *Electrochim. Acta*, 2005, **51**, 1031–1035.
- 17 Q. He, Y. Shen, K. J. Xiao, J. Y. Xi and X. P. Qiu, *Int. J. Hydrogen Energy*, 2016, **41**, 20709–20719.
- 18 P. M. Ejikeme, K. Makgopa, K. Raju and K. I. Ozoemena, *ChemElectroChem*, 2016, **3**, 2243–2251.
- 19 C. W. Xu, Z. Q. Tian, P. K. Shen and S. P. Jiang, *Electrochim. Acta*, 2008, **53**, 2610–2618.
- 20 T. J. Hu, Y. Wang, Q. Liu, L. N. Zhang, H. B. Wang, T. Tang, W. W. Chen, M. Zhao and J. F. Jia, *Int. J. Hydrogen Energy*, 2017, **42**, 25951–25959.
- 21 Y. Z. Su, Q. Z. Xu, Q. S. Zhong, C. J. Zhang, S. T. Shi and C. W. Xu, *Mater. Res. Bull.*, 2015, **64**, 301–305.
- 22 W. Y. Yuan, J. Zhang, P. K. Shen, C. M. Li and S. P. Jiang, *Electrochim. Acta*, 2016, **190**, 817–828.
- 23 J. H. Zhang, T. Zhu, N. Li and C. W. Xu, *J. Energy Inst.*, 2016, **89**, 325–329.
- 24 A. R. Jadhav, H. A. Bandal, A. A. Chaugule and H. Kim, *Electrochim. Acta*, 2017, **240**, 277–287.
- 25 W. Wang, Q. X. Chu, Y. N. Zhang, W. Zhu, X. F. Wang and X. Y. Liu, *New J. Chem.*, 2015, **39**, 6491–6497.
- 26 Z. S. Li, R. R. Yang, B. L. Li, M. Yu, D. H. Li, H. Q. Wang and Q. Y. Li, *Electrochim. Acta*, 2017, **252**, 180–191.
- 27 T. H. Ko, K. Devarayan, M. K. Seo, H. Y. Kim and B. S. Kim, *Sci. Rep.*, 2016, **6**, 20313.
- 28 M. B. Askari and P. Salarizadeh, *J. Mol. Liq.*, 2019, **291**, 111306.
- 29 L. Qian, S. L. Luo, L. S. Wu, X. R. Hu, W. Chen and X. Wang, *Appl. Surf. Sci.*, 2020, **503**, 144306.
- 30 S. N. Sun, Y. Zhou, B. L. Hu, Q. C. Zhang and Z. J. Xu, *J. Electrochem. Soc.*, 2016, **163**, H99–H104.
- 31 J. Zhan, M. Cai, C. F. Zhang and C. Wang, *Electrochim. Acta*, 2015, **154**, 70–76.
- 32 S. S. Jayaseelan, T. H. Ko, S. Radhakrishnan, C. M. Yang, H. Y. Kim and B. S. Kim, *Int. J. Hydrogen Energy*, 2016, **41**, 13504–13512.
- 33 H. X. Gao, Y. Cao, Y. Chen, X. Y. Lai, S. J. Ding, J. C. Tu and J. L. Qi, *J. Alloys Compd.*, 2018, **732**, 460–469.
- 34 B. C. Liu, W. Y. Xia, S. Q. Wang, C. W. Xu and Z. L. Liu, *Int. J. Electrochem. Sci.*, 2018, **13**, 9493–9504.
- 35 N. Benipal, J. Qi, Q. Liu and W. Z. Li, *Appl. Catal., B*, 2017, **210**, 121–130.
- 36 C. C. Jin, J. H. Zhu, R. L. Dong, Z. D. Chen and Q. S. Huo, *Int. J. Hydrogen Energy*, 2016, **41**, 16851–16857.
- 37 C. C. Jin, J. H. Zhu, R. L. Dong and Q. S. Huo, *Electrochim. Acta*, 2016, **190**, 829–834.
- 38 H. B. Wang, L. Thia, N. Li, X. M. Ge, Z. L. Liu and X. Wang, *ACS Catal.*, 2015, **5**, 3174–3180.
- 39 H. J. Kim, S. M. Choi, M. H. Seo, S. Green, G. W. Huber and W. BaeKim, *Electrochem. Commun.*, 2011, **13**, 890–893.
- 40 Y. Y. Li, Z. S. Li and P. K. Shen, *Adv. Mater.*, 2013, **25**, 2474–2480.
- 41 P. K. Sahoo, R. Aepuru, H. S. Panda and D. Bahadur, *Sci. Rep.*, 2015, **5**, 17726.
- 42 N. Arjona, S. Rivas, L. Álvarez-Contreras, M. Guerra-Balcázar, J. Ledesma-García, E. Kjeang and L. G. Arriaga, *New J. Chem.*, 2017, **41**, 1854–1863.

- 43 S. Mao, G. H. Lu and J. H. Chen, *Nanoscale*, 2015, **7**, 6924–6943.
- 44 Y. Y. Li, Q. W. Zhang, J. L. Zhu, X. L. Wei and P. K. Shen, *J. Mater. Chem. A*, 2014, **2**, 3163–3168.
- 45 W. Y. Xia, N. Li, Q. Y. Li, K. H. Ye and C. W. Xu, *Sci. Rep.*, 2016, **6**, 23398.
- 46 L. Gu, L. Qian, Y. Lei, Y. Y. Wang, J. Li, H. Y. Yuan and D. Xiao, *J. Power Sources*, 2014, **261**, 317–323.
- 47 E. Umeshbabu and G. R. Rao, *Electrochim. Acta*, 2016, **213**, 717–729.
- 48 T. H. Ko, S. Radhakrishnan, M. K. Seo, M. S. Khil, H. Y. Kim and B. S. Kim, *J. Alloys Compd.*, 2017, **696**, 193–200.
- 49 H. An, G. H. An and H. J. Ahn, *J. Alloys Compd.*, 2015, **645**, 317–321.
- 50 R. Dinga, L. Qi, M. J. Jia and H. Y. Wang, *Electrochim. Acta*, 2013, **113**, 290–301.
- 51 N. Li, W. Y. Xia, C. W. Xu and S. Chen, *J. Energy Inst.*, 2017, **90**, 725–733.
- 52 C. W. Xu, L. Q. Cheng, P. K. Shen and Y. L. Liu, *Electrochem. Commun.*, 2007, **9**, 997–1001.
- 53 J. F. Gomes and G. Tremiliosi-Filho, *Electrocatalysis*, 2011, **2**, 96–105.
- 54 Y. F. Zhou, Y. Shen, J. Y. Xi and X. L. Luo, *ACS Appl. Mater. Interfaces*, 2019, **11**, 28953–28959.
- 55 R. M. L. M. Sandrini, J. R. Sempionatto, E. Herrero, J. M. Feliu, J. Souza-Garcia and C. A. Angelucci, *Electrochem. Commun.*, 2018, **86**, 149–152.